Advanced Powder Technology 29 (2018) 58–65

Contents lists available at ScienceDirect

Advanced Powder Technology

journal homepage: www.elsevier.com/locate/apt

Original Research Paper

One-step synthesis, characterization and oxidative desulfurization of 12-tungstophosphoric heteropolyanions immobilized on amino functionalized SBA-15

Xuan Nui Pham [a,*], Dinh Linh Tran [a], Tuan Dat Pham [a], Quang Man Nguyen [b], Van Thi Tran Thi [b], Huan Doan Van [c]

[a] Department of Chemical Engineering, Hanoi University of Mining and Geology, 18 Pho Vien, Duc Thang, Bac Tu Liem District, Hanoi, Viet Nam
[b] Department of Chemistry, Hue Science College, Hue University, 77 Nguyen Hue Str., Hue City, Viet Nam
[c] Department of Mechanical Engineering, University of Bristol, Bristol BS8 1TH, United Kingdom

ARTICLE INFO

Article history:
Received 14 July 2017
Accepted 14 October 2017
Available online 31 October 2017

Keywords:
Oxidative desulfurization
Dibenzothiophene
Heteropoly acid
Functional mesoporous materials
One-pot synthesis

ABSTRACT

Keggin-type 12-tungstophosphoric $[PW_{12}O_{40}]^{3-}$ heteropolyanions were successfully immobilized onto mesoporous material surface of SBA-15 functionalized using the (3-aminopropyl)triethoxysilane (APTES) synthesized by one-pot co-condensation method, also called one-step synthesis. The synthesized PW^{-}-NH_3^{+}-SBA-15 catalyst was characterized by XRD, N_2 adsorption–desorption, FT-IR, TGA, SEM, TEM, EDS, XPS methods. The results indicated that ordered hexagonal mesostructure for SBA-15 support was still maintained after being functionalized with amine groups, while the specific surface area of SBA-15 was decreased. The active species of phosphotungstic acid $H_3PW_{12}O_{40}$ (HPW) retained its Keggin structure of the heteropolyanions on the amine-modified SBA-15. The PW^{-}–$^{+}H_3N$–SBA–15 catalyst exhibited a high catalytic activity for oxidative desulfurization process of sulfur-containing model fuel. The dibenzothiophene (DBT) conversion of almost 100% was achieved with reaction conditions of 40 mg of catalyst dosage, 2 mL of hydrogen peroxide, 90 °C of reaction temperature, and 120 min of reaction time.

1. Introduction

Organic compounds containing sulfur in fuels are the major source of pollution. Emission of SO_x from vehicle engine causes acid rain, engine and pipeline corrosions, and catalysts poison in the catalytic processes. Hence, the stringency of environmental regulations drives the maximum reduction of sulfur content in fuel. For example, that content in the diesel in Europe and the United States must be reduced to less than 10 and 15 ppmw, respectively [1]. To meet this requirement, many methods have been applied in the field of deep – desulfurization.

Currently, conventional hydrodesulfurization (HDS) technology has been applied to remove sulfur from the liquid fuel. However, this technology requires the strict operating conditions, and takes place in the reactor at high temperature (300–400 °C), high pressure (3–6 Mpa), and in the presence of hydrogen [2]. Although it is effective method for the removal of sulfur-containing cyclic and aliphatic hydrocarbons, it has exhibited some inherent problems in treating sulfur-containing aromatic hydrocarbon compounds such as dibenzothiophene (DBT), benzothiophene (BT) and their derivatives as the existence of benzene rings in molecular enhances their aromatic [3–5].

In order to overcome this drawback, many other technologies have been applied such as oxidative desulfurization (ODS) [6–8], adsorptive desulfurization [9], extraction by ionic liquids [10,11], biodesulfurization [12].

Up to now, there are many studies on the use of appropriate catalysts for sulfur removal by the oxidation [13–19]. Among the oxidation methods applied, oxidative desulfurization on the base of tungsten as active species is one of the promising ways complement HDS due to its mild operating conditions e.g.atmospheric pressure, no consumption of hydrogen, and high efficiency. Under this process, sulfur-containing compounds can be selectively oxidized to sulfoxides or sulfones in the presence of hydrogen peroxide as oxidative agent. The formation of sulfone and sulfoxide compounds with the polar bonds of sulfur-oxygen (S═O), resulting

* Corresponding author.
E-mail address: phamxuannui@humg.edu.vn (X.N. Pham).

https://doi.org/10.1016/j.apt.2017.10.011
0921-8831/

in their solubility in polar solvents and their extractability in non-polar organic solvent [20].

Recently, several research groups have developed silica supported active tungsten species for oxidative desulfurization, such as W-MCM-41 [15], silica supported $H_3PMo_{12}O_{40}$ [19] synthesized by direct one-pot method, MCM-41 supported $(Bu_4N)_4H_3(PW_{11}O_{39})$ [16], silica supported $[(n\text{-}C_8H_{17})_3NCH_3]_2W_2O_{11}$] [21]. Li et al. [22] reported the using decatungstates $[(C_4H_9)_4N]_4W_{10}O_{32}$ in the ionic liquid of $[Bmim]PF_6$ catalyzed for deep oxidative desulfurization of fuel oils.

Keggin structure type 12-tungstophosphoric heteropolyacid $H_3PW_{12}O_{40}$ (HPW) is promising catalytic material because their superacid properties with strong Bronsted acid sites, high proton mobility, redox activity, high thermal stability, and environmental friendliness [23–25]. Polyoxometalate catalyst has been used for oxidative desulfurization [26]. However, pure HPW materials as the catalysts are hindered by their low specific surface area (<10 m^2/g), and high solubility in polar solvents in reaction system which leads to the difficulty of catalysts recovery [27].

Immobilization of HPW by supporting HPW onto a solid porous substrate such as amorphous silica [28–30], carbon nanotubes [31] etc. is one of effective methods to increase the surface area, and to separate and recycle the catalysts [32]. Among the porous substrates, mesoporous SBA-15 is very interesting material due to its large specific surface area allowing exellent dispersion of catalytic active sites. Further, the large pore size of that material can aid the movement of bulky organic molecules in and out of the pores.

In this work, we present a direct synthetic method to prepare the amino-functionalized SBA-15 by using (3-aminopropyl) triethoxysilane (APTES) introduced into mesoporous silica in the presence of triblock copolymer Pluronic P123 as a structure directing agent. The HPW catalyst was immobilized on the surface of amino-functionalized ordered mesoporous SBA-15 (H_2N-SBA-15) by using triflic acid as the protonated agent. The HPW catalyst immobilized on the NH_2–SBA-15 silica were characterized by various physicochemical methods. The ability of this catalyst to facilitate the oxidative desulfurization process was tested using dibenzothiophene as model oil with H_2O_2 oxidant. The operating conditions, including the reaction temperature, H_2O_2 dosage, and catalyst dosage were investigated.

2. Experimental

2.1. Materials

Dibenzothiophen (DBT, 99%), 3-aminopropyltriehoxysilane (APTES, 99%), triblock copolymer Pluronic P123 [poly (ethylene glycol)-block-poly (propylene glycol)-block-poly (ethylene glycol) ($EO_{20}PO_{70}EO_{20}$) (M = 5750) were purchased from Sigma–Aldrich. Tetraethyl orthosilicate (TEOS, 99%) were purchased from Merck. $H_3PW_{12}O_4{\cdot}14H_2O$ (HPW, AR grade), triflic acid (AR grade); *n*-octane (AR grade), hydrogen peroxide (H_2O_2, 30% AR grade), hydrochloric acid (HCl, 37% AR grade) were purchased Sinopharm Chemical Reagent Beijing Co., Ltd. (Beijing, China). All other used solvents were obtained from commercial sources and used as received or distilled and dried using standard procedures.

2.2. Preparation of amine-modified SBA-15 (H_2N-SBA-15) by the co-condensation method

In a typical synthesis, 4 g of Pluronic P123 was dissolved in 160 mL of 2 N HCl solution. Then 8.5 g of tetraethyl orthosilicate (TEOS) was added into the mixture above. The mixture was continuously stirred at 45 °C for 3 h before the addition of 0.95 g of 3-aminopropyltriehoxysilane (APTES). After stirring for 24 h at 45 °C, the final mixture was transferred to a Teflon-lined stainless steel atoclave for hydrothermal synthesis at 110 °C for 24 h. The solid product synthesized was collected, washed by distilled water, dried overnight at 80 °C, and calcined at 550 °C for 6 h with the heating rate of 5 °C/min. The obtained sample was designated as H_2N-SBA-15 (M4).

2.3. The immobilization of HPW onto the NH_2–SBA-15 silica support ($PW^-H_3N^+$-SBA-15)

To increase the immobilization of HPW onto surface of H_2N-SBA-15 material, in this study, triflic acid was used as the reagent protonating amine groups to create positively charged NH_3^+ groups on the support. As the result, there is the formation of electrostatic interaction between NH_3^+ of support surface with $PW^-$of HPW. Immobilization of HPW on H_2N-SBA-15 silica support was carried out as follows [33]: 1 g of H_2N-SBA-15 was suspended in 50 mL of acetonitrile solvent, then 4 mL of triflic acid solution was added into the reaction mixture and refluxed at 80 °C for 5 h. After that the solid product was filtered, and was washed with acetonitril to remove the unreacted triflic acid. The acidified H_2N-SBA-15 obtained was designated as ^+H_3N-SBA-15. Immobilization of HPW catalyst on H_2N-SBA-15 support was performed by adding of 0.7 g of ^+H_3N-SBA-15 into mixture containing 50 mL methanol and 0.3 g of HPW. The mixture was refluxed at 65 °C for 5 h before being filtered to obtain solid product, which was dried under vacuum in an oven at 100 °C overnight. The product sample is designated as PW^-–^+H_3N–SBA–15.

2.4. Characterization

X-ray diffraction patterns of the solid powders were recorded on a D8-Advance Bruker with Cu-Kα radiation (λ = 1.5406 nm). N_2 adsorption–desorption isotherms were measured by a TriStar 3000 (Micromeritics). Surface areas were calculated from the linear part of the BET plot. Pore size distributions were calculated using the adsorption branches of the N_2 isotherms and the Barret-Joyner-Halenda (BJH) method. Scanning electron microscopy (SEM) images and energy-dispersive X-ray spectroscopy analysis (EDAX) were taken on a JED-2300. The images of TEM were taken by a JEM-1010 (Jeol, Japan) operated at an accelerating voltage of 200 kV. Infrared data were examined by a Shimadzu IR Prestige-21 spectro-meter (Japan) using KBr pallets. TGA and DTA were performed by using a TG Setaraminstrument (France) in the argon gas (100–1000 °C). XPS spectra were taken by an AXISULTRA DLD Shimadzu Kratos spectrometer (Japan) using monochromated Al K_α radiation (1486.6 eV).

2.5. Oxidative desulfurization process

Model fuel samples with a corresponding S-content of 500 ppm were prepared by dissolving dibenzothiophene (DBT) in *n*-octane. The reaction was carried out in a 100 mL three-neck flask, with a reflux condenser, placing on a magnetic stirrer. In a typical run using H_2O_2 as oxidative agent, an appropriate amount of catalysts was added with constant stirring under the right temperature.

After collecting about 1 mL product solution samples and centrifuging every 30 min, samples were analyzed by HPLC Series 20A system (Shimadzu, Japan) under analytic conditions with X-Bridge C18 Column (25 cm × 4 mm × 5 μm), Waters, Ireland and Acetonitrile/H_2O ratio equal to 70/30 (v/v). The UV Detector was installed at the wavelength of 315 nm for dibenzothiophene. The flow rate was at 1.3 mL/min. The volume of injected sample was 10 μl.

The intermidate products of reaction were analyzed by a Gas Chromatograph–Mass Spectrometer (GC–MS) (Agilent

7890/5975C-Gas Chromatography (GC)/Mass Selective Detector (MSD), HP-5 MS column, 30 m × 0.25 mm × 0.25 μm. The temperature was set at 100 °C temperature and rised at the rate of 15 °C/min to 200 °C for 10 min.

3. Results and discussion

3.1. Structural characterization of mesoporous H_2N-SBA-15 supported 12-tungstophosphoric acid catalyst (PWH_3N^+–SBA–15)

Fig. 1 shows XRD patterns of SBA-15, H_2N-SBA-15, and PW^-–NH_3^+–SBA–15 samples synthesized by direct one–step method.

In the XRD result of SBA-15 support, there are reflections with *hkl* indexes (1 0 0), (1 1 0), and (2 0 0) at 2θ = 0.91°, 1.56°, and 1.76°, respectively. These peaks are typical for the *P6mm* hexagonal structure of SBA-15 support [34]. In comparison, H_2N-SBA-15 and PW^-–NH_3^+–SBA–15 samples have lower peak at (1 0 0) and ill-resolved peaks at (1 1 0) and (2 0 0), demonstrating that the ordering of the mesostructure decreases. This phenomenon could be due to the organic groups of APTES perturb the self-assembly of surfactant micelles and the silica precursors [35]. It is also noticed that the positions of the (1 0 0) peaks slightly shift to smaller angles (2θ = 0.8) in the XRD spectrum of H_2N-SBA-15, PW^-–NH_3^+–SBA–15 samples. This proves that amino-functionalized SBA-15 samples have the unit cell d_{100} spacing increases compared to the original SBA-15.

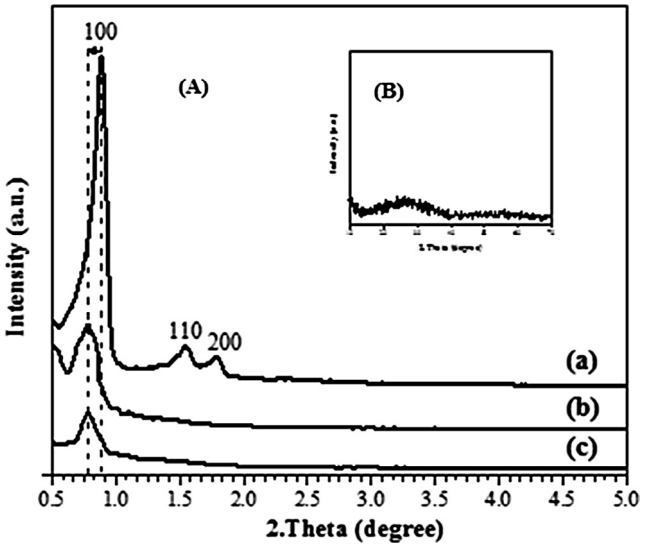

Fig. 1. (A) Low-angle XRD patterns of SBA-15 (a), H_2N-SBA-15 (b), PW^--H_3N^+-SBA-15 (c) samples, and (B) Wide-angle XRD pattern of PW^--H_3N^+-SBA-15 sample.

Fig. 1(B) shows the wide-angle XRD patterns of the PW^--H_3N^+-SBA-15 catalyst. This pattern is the typical one for amorphous pore walls SBA-15 with a broad halo at 2θ = 25°. Crystalline pattern of HPW was not observed at wide angle. Furthermore, the absence of characteristic peaks of crystalline phase of TPW indicates that HPW was anchored of SBA-15.

The SEM-EDX image (Fig. 2a) of PW^--NH_3^+-SBA–15 exhibited a fiber-like unform cylindrical morphology, which is in good agreement with the typical SBA-15 morphology [36]. The composition of PW^--H_3N^+-SBA-15 sample was estimated using EDX analysis (Fig. 2b). It can be shown that the amount of W containedin sample was 20.89 %wt.

Fig. 3(a) and (b) show TEM images of SBA-15 and PW^--NH_3^+-SBA–15, respectively. It can be seen that these mesoporous silica materials exhibited an ordered mesostructure with the hexagonal ordered arrays of on dimensional mesoporous material.

Fig. 4 shows the FT-IR spectra of SBA-15, H_2N-SBA-15, PW^--H_3N^+–SBA–15, and HPW samples. The peaks at 1051.20, 802.39, and 424.34 cm^{-1} is assigned to the asymmetric and symmetric stretching vibration of Si—O—Si bridge, the absorption band at 972 cm^{-1} represents the Si—O—Si or Si—OH in plane stretching vibration of silanol groups in the framework of SBA-15 [37]. An increase in the intensity of the absorption band at 1622.13 cm^{-1} (Fig. 4b and c), which correspond not only for physically absorbed water molecules on silica surface but also to an overtone of the N—H blending vibration that indicate the presence of primary amine groups [38]. Characteristic IR spectra of the bulk HPW acid and PW^--H_3N^+–SBA–15 in the region from 1100 to 700 cm^{-1} (Fig. 4c and d) are attributed to Keggin type structure, the band at 1074.35 cm^{-1} are assigned to the asymmetry vibrations of the oxygen atom bonded to phosphorous in the central PO_4 unit. The band at about 958.62 cm^{-1} correspond to stretching vibrations of W=O, and the adsorption band appeared at 881.47 cm^{-1} was attributed to the asymmetry vibrations W—O—W in Keggin anion structure PW^- [39]. It can be clearly seen that the vibration bands of PW^--H_3N^+–SBA–15 are similar to those of the corresponding bulk PW^-, suggesting that the Keggin structure remained intact after anchoring on the mesoporous SBA-15 surface.

The nitrogen adsorption–desorption isotherms of the SBA-15, H_2N-SBA-15, and PW^-–NH_3^+–SBA–15 catalysts were depicted in Fig. 5A. All the isotherms were the type IV in nature according to the IUPAC classification and exhibited the H1 hysteresis loops, indicating the characteristic of mesoporous solids [40]. Furthermore, the adsorption branches of all the isotherms showed a sharp inflection at at a quite high relative pressure (P/P_o = 0.62) indicat-

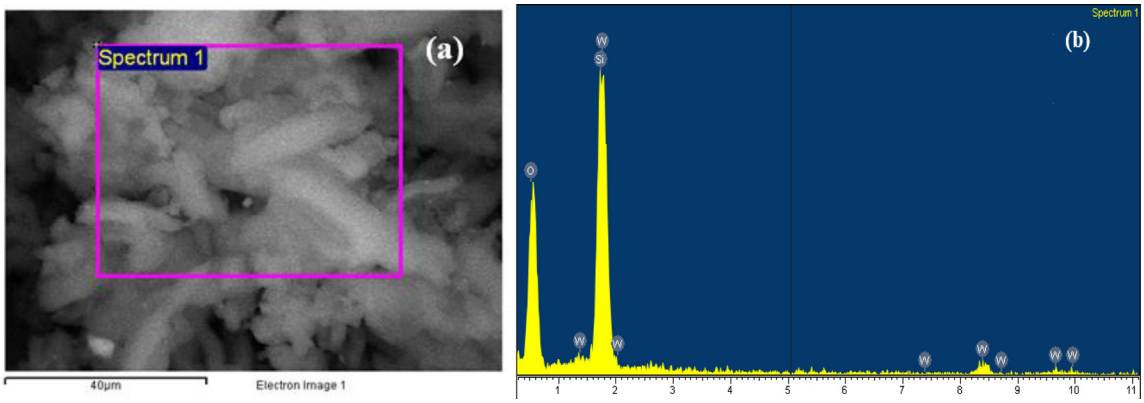

Fig. 2. SEM (a) and EDX (b) results of PW^--NH_3^+-SBA–15 catalyst.

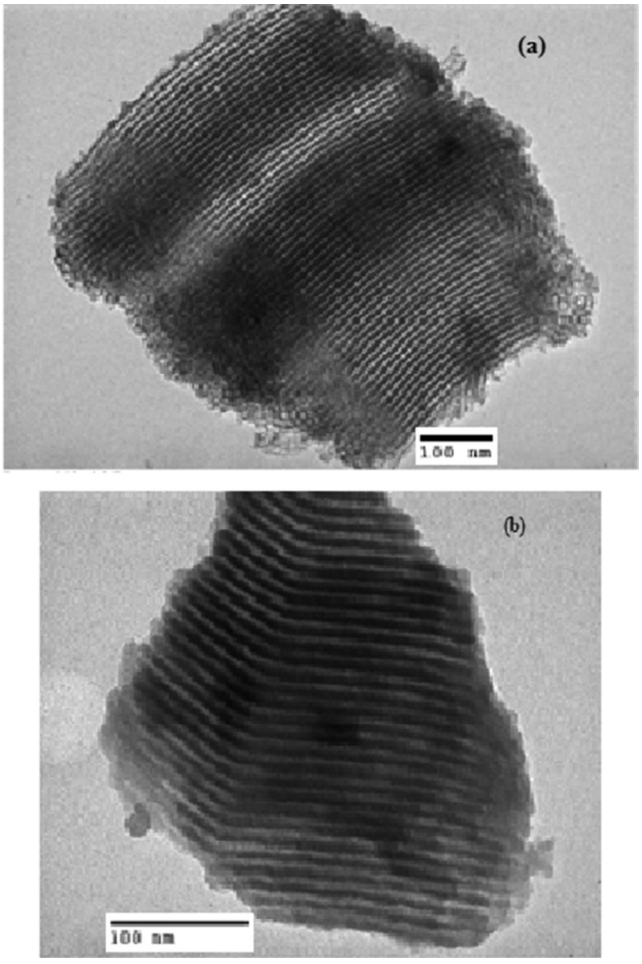

Fig. 3. TEM images of SBA-15 support (a) and PW^{-}-NH_3^+-SBA–15 catalyst (b).

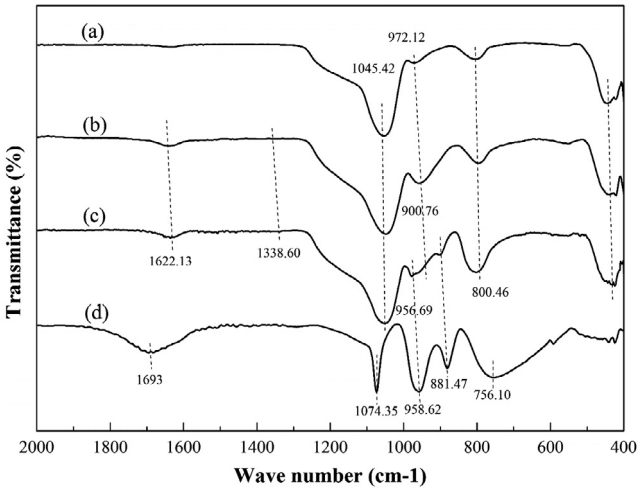

Fig. 4. FT-IR spectra of SBA-15 (a), H_2N-SBA-15 (b), PW^{-}–NH_3^+–SBA–15 (c), and HPW (d) samples.

ing the typical capillary condensation within uniform pores. The physicochemical parameters of samples, such as the BET area (S_{BET}), pore volume (V_p), pore diameter (D_p) are listed in Table 1. It was found that SBA-15 exhibited hight surface area (593.73 $m^2\ g^{-1}$) and the surface areas of the H_2N-SBA-15, PW^{-}–NH_3^+–SBA–15 catalysts were about 507.42, 449.82 $m^2\ g^{-1}$, respectively. After immobilization of the Keggin units in H_2N-SBA-15, a decrease in the surface area and total pore volume was observed. Similar results were also performed by Castanheiro et al. [41].

Fig. 5B shows the pore size distributions of SBA-15, H_2N-SBA-15 and the typical PW^{-}–NH_3^+–SBA–15 catalysts. Pore diameter and pore volume calculated from the N_2 desorption data based on the BJH method. For H_2N-SBA-15 and PW^{-}–NH_3^+–SBA–15 catalyst samples have pore sizes of approximately 4.5 nm is smaller than SBA-15 support (6.86 nm). It could be seen though the decrease in the relative pressure for capillary condensation, as well as the amount of nitrogen gas adsorbed was observed for H_2N-SBA-15 and PW^{-}-H_3N^+-SBA-15 samples. For SBA-15 support, the capillary condensation phenomenon occurred at $P/P_o = 0.62$ and adsorbed gas volume of 270 cm^3/g. In addition, H_2N-SBA-15 and PW^{-}-H_3N^+-SBA-15 catalyst samples, however, the relative pressure for capillary condensation was approximately at 0.4, and N_2 gas adsorption was 180 cm^3/g for H_2N-SBA-15 and 120 cm^3/g for PW^{-}-H_3N^+-SBA-15 catalyst, which indicate that the aminization by APTES and immobilization of PW^{-} inside the mesopores of SBA-15 significantly reduced the volume of the pores. This result is similar to previous research by M. Zhang et al. [15]. The space distance between (*1 0 0*) planes and the values of hexagonal unit-cell parameter (a_o), and wall thickness (w) of mesotructure were indetical for all samples, as showed in Table 1. In these case, the interplanar spacing (d_{100}), unit-cell parameter (a_o), and wall thickness (w) of H_2N-SBA-15, PW^{-}-H_3N^+-SBA-15 catalyst samples determined in the range of 11.4, 8.77, 8.77 nm, respectively. The wall thickness of the SBA-15, obtained by the difference betweenthe interplanar spacing (d_{100}) and unit cell parameter (a_o), was of 4.66 nm. The increase in the wall thickness was due to the aggregation of the APTES molecule with precursor substance of tetraethyl orthosilicate in the one-pot synthesis process of amino-functionalized SBA-15.

To calculate the amount of amine–modified mesoporous materials và PW^{-} anchored into H_2N–SBA–15, the TG analysis were performed as shown in Fig. 6. For SBA-15 support (Fig. 6a), the weight loss at below 100 °C is due to the removal of physically adsorbed water, while the weight loss in the range of 100–700 °C is associated with the decomposition of the surfactant in the pores. The weight loss at about 700 °C is a result of surface silanol condensation to form siloxane (≡Si—OH) [42]. For H_2N-SBA-15 sample (Fig. 6b) shows the mass loss of 13.83% in the temperature range of 200–700 °C corresponding to the decay of APTES inside the channels pores.

Fig. 6c, the weight loss of PW^{-}-H_3N^+-SBA-5 catalyst samples in the range of 200–800 °C corresponds to the temperature range of decomposition of the PW^{-} and APTES with the presence of triflic acid on the surface. The decomposition rate of PW^{-} obtained is 9.74% lower than that of APTES indicating the presence of PW-inside the pore channels of SBA-15.

The XPS spectra shown in Figs. 7 and 8 give the information of chemical state and the weight of the compound on the outer surface of H_2N–SBA–15 and PW^{-}-H_3N^+-SBA-15, respectively. The wide XPS scan spectra (Figs. 7 and 8a) shows that C 1s element with binding energy of 284.8 eV exists on the surface of the materials. The weak signal of N 1s at 400.2 eV was also observed. The binding energy of O 1s appears at the range of 529–530 eV showing that oxygen exists in the form of metal oxide. The binding energy of Si 2p and Si 2s from silicon dioxide is 103.5 eV and 161.4 eV, respecsively. Beside, XPS spectrum of PW^{-}-H_3N^+-SBA-15 sample show that two overlapped peaks in W 4f region (Fig. 8b) corresponding to W $4f_{7/2}$ and $4f_{5/2}$ with the binding energy of 36.1 and 38.2 eV, repectively, are obtained. That means the oxidization states/coordination environments correspond to the form of W^{6+}—O—Si and W^{6+}—O—W [43–45]. The different between two XPS maximum signals of W $f_{7/2}$ and W $f_{5/2}$ is about 2 eV. It can

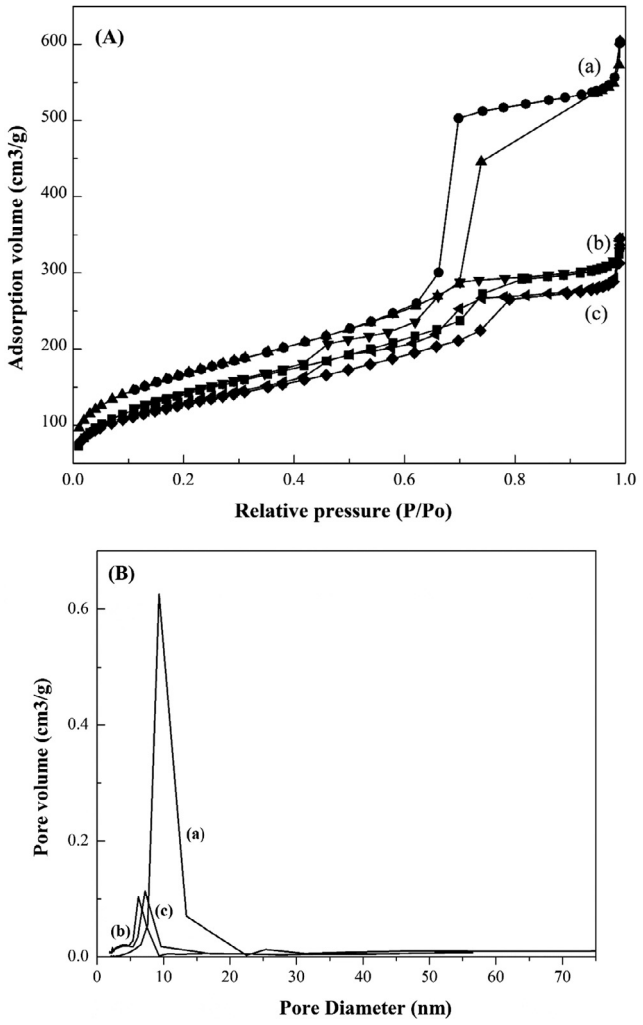

Fig. 5. N_2 adsorption–desorption isotherm (A) and pore size distribution (B) of the SBA-15 (a), H_2N-SBA-15 (b), and PW^{-}-H_3N^{+}-SBA-15 (c).

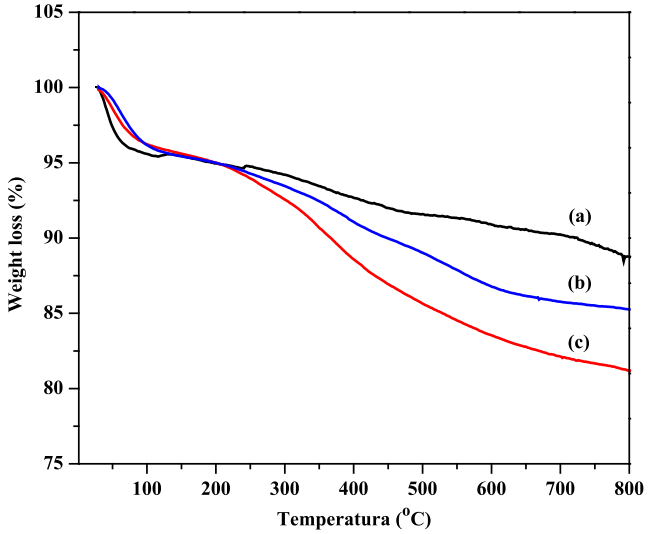

Fig. 6. Thermal analysis curves (TG) of pure SBA-15 (a), H_2N–SBA–15 (b), PW^{-}-NH_3^{+}-SBA–15 (c).

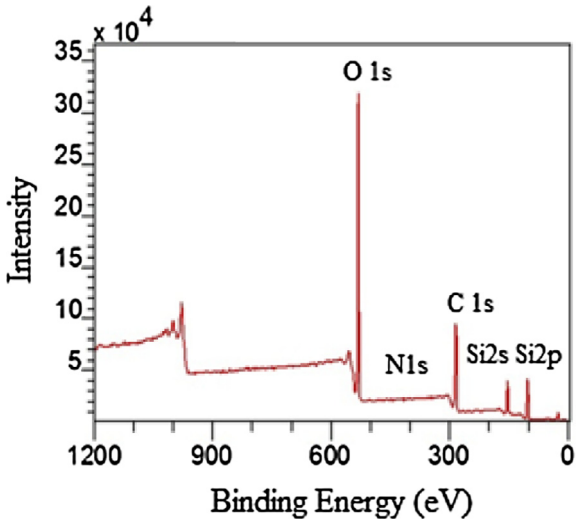

Fig. 7. XPS pattern of H_2N-SBA-15.

be inferred to the presence of WO_3 on SBA-15 surface. The loss of W metal sign at the binding energy of 42 eV was measured due to the cover of WO_3 4f symmetry peak. Thus, it can be concluded that PW^{-} was successfully mounted on the surface of SBA-15 via an amine bridge protonated.

3.2. Catalytic activity test

The effect of the reaction conditions including temperature and reaction time, dosage of catalyst, and the dosage of H_2O_2 as an oxidizing agent have been investigated over PW^{-}- H_3N^{+}-SBA-15 catalyst for the oxidative desulfurization of DBT. the oxidative desulfurization of DBT in model fuel was carried out with the catalyst dosage of 0.04 g, H_2O_2 amount of 2 mL, and the volume of model fuel was 20 mL.

To explore the effect of the reaction temperature on catalytic oxidation of DBT by PW^{-}- H_3N^{+}-SBA-15 catalyst, the reactions under various temperatures were carried out. As shown in Fig. 9, the DBT conversion efficiencies at 50, 70, and 90 °C were estimated

Table 1
Textural and structural characteristics of SBA-15, H_2N-SBA-15, and the PW^{-}-NH_3^{+}-SBA–15 catalysts.

Sample	S_{BET} (m^2g^{-1})	V_p (cm^3g^{-1})	D_p (nm)	d_{100} (nm)	a_o (nm)	w (nm)
SBA–15	593.73	0.93	6.86	9.98	11.52	4.66
H_2N-SBA-15	507.42	0.40	4.39	11.40	8.77	8.77
PW^{-}-NH_3^{+}-SBA–15	449.82	0.38	4.50	11.40	8.64	8.64

Specific surface area calculated by the BET method (S_{BET}).
The pore diameter (D_p) and pore volume (V_p) calculated from the N_2 desorption data based on the BJH method.
d_{100}, the space distance between (*1 0 0*) planes.
a_o, lattice cell parameter of the hexagonal structure.
Unit-cell parameter determined from the position of the (*1 0 0*) diffraction line as $a_o = 2d_{100}\sqrt{3}$.
Pore wall thickness calculated as $w = a_o - D_p$.

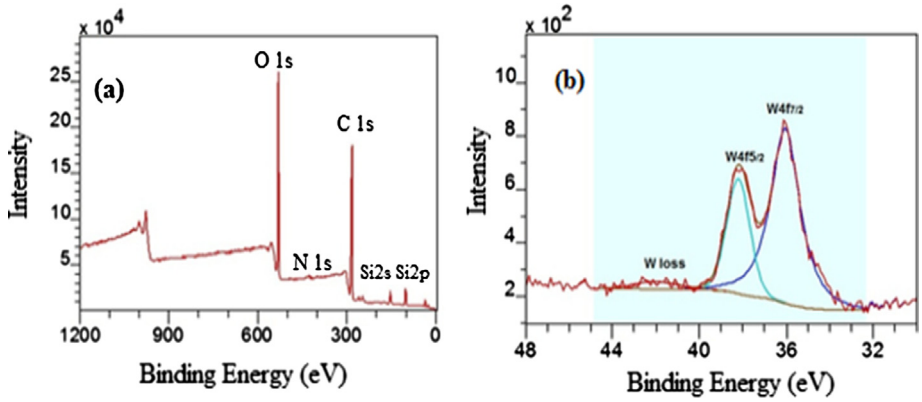

Fig. 8. XPS patterns (a) and W 4f core level spectrum (b) of PW^{-}-H_3N^{+}-SBA-15.

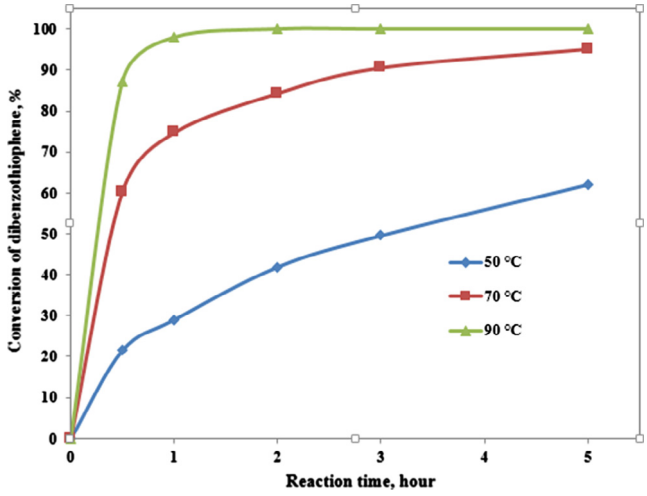

Fig. 9. Effect of the reaction temperature on the conversion of DBT. Experimental conditions: $V_{model\ oil}$ = 20 mL; $m_{catalyst}$ = 40 mg; V_{H2O2} = 2 mL.

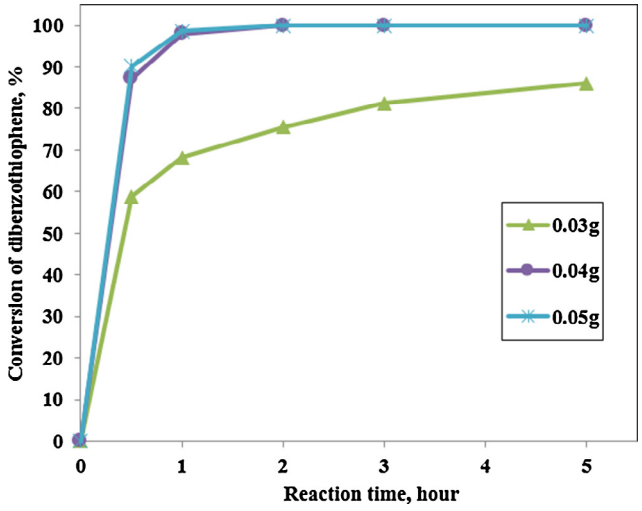

Fig. 10. Effect of the dosage of catalyst on the conversion of DBT in different reaction time. Experimental conditions: $V_{model\ oil}$ = 20 mL; $m_{catalyst}$ = 40 mg; V_{H2O2} = 2 mL.

to be 21.53%, 60.36%, and 87.29%, respectively, after the reaction for 30 min. The results show that the reaction temperature increased from 70 to 90 °C resulted in a faster oxidation rate. When the temperature was further increased to 90 °C, the highest conversion of DBT of 100% was observed after 120 min, and this conversion was still unchanged during the reaction time of 300 min, which may be attributed to the rapid decompositions of hydrogen peroxide to form the active phase of intermediate tungsten peroxo coordination, $W(O_2)_n$, in the presence of monovacant Keggin unit [46] resulting the desulfurization rate reaches the maximum (100%). While the DBT conversion increased with increasing of reaction time at lower reaction temperature. The highest conversion (95.22%) occurred when reaction time and temperature were set at about 300 min and 70 °C, respectively. Hence, the optimal reaction temperature was eventually set to 90 °C.

A proper selection of catalyst dosage was crucial to have the maximum ODS efficiency at the minimum consumption of catalyst. The oxidative desulfurization of DBT in model fuel was carried out at 90 °C, and the different reaction conditions are similar to the above. A series dosage of fresh catalsyst PW^{-}- H_3N^{+}-SBA-15 ranging from 0.02 to 0.04 g. From Fig. 10, as the catalyst dosage increased from 0.03 to 0.04 g, the conversion of DBT increased fast from 58.84% to 87.29% was observed within 30 min. Along with this time, the conversion of DBT increased slightly from 87.29% to 90.212% when the catalyst dosage increased from 0.04 to 0.05 g, respectively, and the conversion of the both catalysts reaches

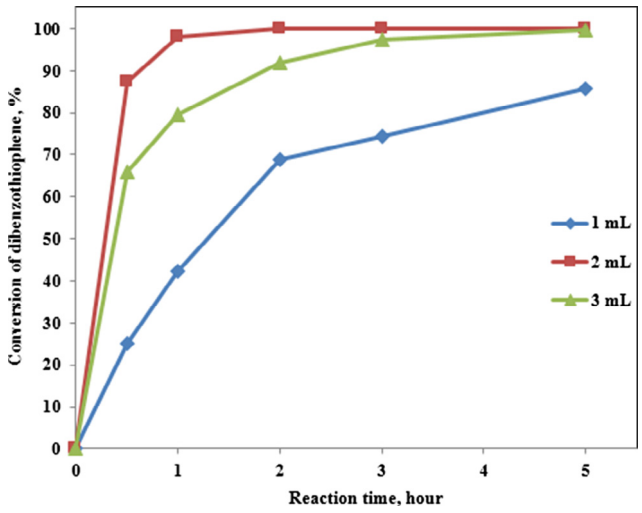

Fig. 11. Effect of H_2O_2 amount on the conversion of DBT. Experimental conditions: $V_{model\ oil}$ = 20 mL; $m_{catalyst}$ = 40 mg; V_{H2O2} = 2 mL.

100% after reaction time of 120 min. From the obtained results reveal that increasing the catalyst dosage could enhance the oxidative desulfurization of DBT due to the catalytic active sites in the

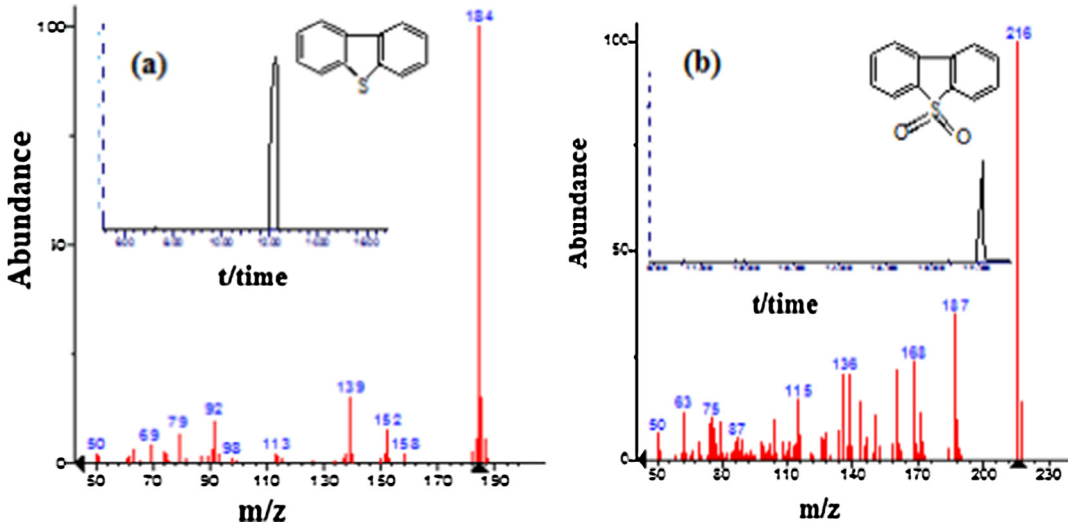

Fig. 12. The GC–MS of DBT (a), and $DBTO_2$ (b).

catalyst systems are enriched. However, when further increasing catalyst dosage up to 0.05 g, no appreciable change was discovered on the conversion of DBT, which indicate that catalytic activity is not able to improve significantly, perhaps because the most DBT was oxidized in the first stages of the reaction with the increasing of the number reactive sites. Thus, 0.04 g was preferable for the catalyst dosage.

Fig. 11 displays the removal of DBT under different H_2O_2 amount. The results show that an increase in the H_2O_2 amount from 1 to 2 mL resulted in a superior DBT conversion efficiency (from 25.23% to 87.29%) after 30 min, the actual 2 mL of H_2O_2 for the complete conversion of DBT (100%) after 120 min. However, when the amount of H_2O_2 was greater than 2 mL the desulfurization ratesdecreased obviously (91.95%) after 120 min, which may be related to the H_2O_2 dosage increased leads to the decomposition rate increasing of H_2O_2, hence, the concentration of H^+ in the catalytic systems also increased which strengthened the attack of the proton (H^+) to oxygen atom of W=O species and prevented the formation of intermediate states of $W(O_2)_n$ peroxotungstate species. Therefore, the formation quantity of the hydroperoxytungstate species decreased and the oxidative desulfurization activity of DBT fell down [17].

Fig. 12 shows the results of GC–MS analysis of oxidation reaction of DBT to sulfone (DBT-O_2). It is found that there are no peaks of DBT detected in the product sample collected after 120 min of reaction time (Fig. 12b). Mass spectrum of the product showed the strongest peak of molecular ion with $m/z = 216$ belonging to $DBTO_2$, which is a product of DBT oxidation reaction. From the results obtained above, it can be pointed out that DBT was adsorbed and oxidized on PW^-- H_3N^+-SBA-15 in the presence of oxidizing agent (H_2O_2). The polar products are separated by polar solvents for the deep reduction of sulfur to obtain clean fuels.

4. Conclusions

The ordered-mesoporous material, H_2N-SBA-15, functionalized with (3-aminopropyl)triethoxysilane (APTES) was successfully synthesized by using one-stage synthetic method, in which the Keggin 12-tungstophosphoric heteropolyanion (HPW^-) was immobilized onto functionalized H_2N-SBA-15 material. The results obtained by FT-IR, XPS, EDX-SEM, and wide angle XRD confirmed the appearance of HPW on the surface of mesoporous silica material, while the results of small angle XRD, N_2 isotherms, and TEM prove that the structure of the mesoporous material was maintained. The synthesized heterogeneous PW^--NH_3^+-SBA-15 catalyst has high catalytic activity for the oxidative desulfurization reaction of DBT, with the conversion of DBT in H_2O_2 reached 100% in 120 min.

Acknowledgement

The authors gratefully acknowledge the financial supports by the National Foundation for Science and Technology Development (NAFOSTED) of Vietnam (Grant No. 105.99-2015.21).

Appendix A. Supplementary material

Supplementary data associated with this article can be found, in the online version, at https://doi.org/10.1016/j.apt.2017.10.011.

References

[1] C. Song, An overview of new approaches to deep desulfurization for ultra-clean gasoline, diesel fuel and jet fuel, Catal. Today 86 (2003) 211–263.
[2] Z.C. Shao, H. Nie, X.D. Gao, Effect of nitrogen-containing compounds on deep and ultradeep HDS for diesel oil. II Effect of Processing Conditions and Catalyst. Acta Petrolei Sinica (Petroleum Processing Section) 22(5) (2006) 14–19.
[3] C. Song, X.L. Ma, New design approaches to ultra-clean diesel fuels by deep desulfurization and deep dearomatization, Appl. Catal. B: Environ. 41 (2003) 207–238.
[4] M. Houalla, D.H. Broderick, A.V. Sapre, N.K. Nag, V.H.J. de Beer, B.C. Gates, H. Kwart, Hydrodesulfurization of methyl-substituted dibenzothiophenes catalyzed by sulfided Co-Mo/γ-Al_2O_3, J. Catal. 61 (1980) 523–527.
[5] Z. Deng, T. Wang, Z. Wang, Hydrodesulfurizationof diesel in a slurry reactor, Chem. Eng. Sci. 65 (2010) 480–486.
[6] J.M. Campos-Martin, M.C. Capel-Sanchez, P. Perez-Presas, J.L.G. Fierro, Oxidative processes of desulfurization of liquid fuels, J. Chem. Technol. Biotechnol. 85 (2010) 879–900.
[7] Si.W. Li, R.M. Gao, R.L. Zhang, J.S. Zhao, Template method for a hybrid catalyst material POM@MOF-199 anchored on MCM-41: Highly oxidative desulfurization of DBT under molecular oxygen, Fuel 184 (2016) 18–27.
[8] W. Zhu, G. Zhu, H. Li, Y. Chao, Y. Chang, G. Chen, C. Hana, Oxidative desulfurization of fuel catalyzed by metal-based surfactant-type ionic liquids, J. Mol. Cat. A Chem. 347 (2011) 8–14.
[9] R.T. Yang, A.J. Hernández-Maldonado, F.H. Yang, Desulfurization of transportation fuels with zeolites under ambient conditions, Science 301 (2003) 79–81.
[10] F. Li, R. Liu, J. Wen, D. Zhao, Z. Sun, Y. Liu, Desulfurization of dibenzothiophene by chemical oxidation and solvent extraction with $Me_3NCH_2C_6H_5Cl.2ZnCl_2$ ionic liquid, Green Chem. 11 (2009) 883–888.
[11] J. Eßer, P. Wasserscheid, A. Jess, Deep desulfurization of oil refinery streams by extraction with ionic liquids, Green Chem. 6 (2004) 316–322.
[12] M. Soleimani, A. Bassi, A. Margaritis, Biodesulfurization of refractory organic sulfur compounds in fossil fuels, Biotechnol. Adv. 25 (2007) 570–596.

[13] G. Rodriguez-Gattorno, A. Galano, E. Torres-García, Surface acid-basic properties of WO_x–ZrO_2 and catalytic efficiency in oxidative desulfurization, Appl. Catal. B 92 (2009) 1–8.
[14] A. Sattler, G. Parkin, Carbon−sulfur bond cleavage and hydrodesulfurization of thiophenes by tungsten, J. Am. Chem. Soc. 133 (11) (2011) 3748–3751.
[15] M. Zhang, W. Zhu, H. Li, S. Xun, W. Ding, J. Liu, Z. Zhao, Q. Wang, One-pot synthesis, characterization and desulfurization of functional mesoporous W-MCM-41 from POM-based ionic liquids, Chem. Eng. J. 243 (2014) 386–393.
[16] Z.E.A. Abdalla, B. Li, Preparation of MCM-41supported $(Bu_4N)_4H_3(PW_{11}O_{39})$ catalyst and its performance in oxidative desulfurization, Chem. Eng. J. 200–202 (2012) 113–121.
[17] J.L. García-Gutiérrez, G.C. Laredo, P. García-Gutiérrez, F. Jiménez-Cruz, Oxidative desulfurization of diesel using promising heterogeneous tungsten catalysts and hydrogen peroxide, Fuel 138 (2014) 118–125.
[18] H. Mirhoseini, M. Taghdiri, Extractive oxidation desulfurization of sulfur-containing model fuel using hexamine–phosphotungstate hybrid as effective heterogeneous catalyst, Fuel 167 (2016) 60–67.
[19] J. Qiu, G. Wang, Y. Zhang, D. Zeng, Y. Chen, Direct synthesis of mesoporous $H_3PMo_{12}O_{40}/SiO_2$ and its catalytic performance in oxidative desulfurization of fuel oil, Fuel 147 (2015) 195–202.
[20] G. Zhang, F. Yu, R. Wang, Research advances in oxidative desulfurization technologies for the production of low sulfur fuel oils, Petrol. Coal 51 (3) (2009) 196–207.
[21] Q. Gu, W. Zhu, S. Xun, Y. Chang, J. Xiong, M. Zhang, W. Jiang, F. Zhu, H. Li, Preparation of highly dispersed tungsten species within mesoporous silica by ionic liquid and their enhanced catalytic activity for oxidative desulfurization, Fuel 117 (2014) 667–673.
[22] H. Li, X. Jiang, W. Zhu, J. Lu, H. Shu, Y. Yan, Deep oxidative desulfurization of fuel oils catalyzed by Decatungstates in the Ionic liquid of $[Bmim]PF_6$, Ind. Eng. Chem. Res. 48 (2009) 9034–9039.
[23] A.C. Estrada, M.M.Q. Simões, I.C.M.S. Santos, M.G.P.M.S. Neves, A.M.S. Silva, J.A. S. Cavaleiro, A.M.V. Cavaleiro, Iron-substituted polyoxotungstates as catalysts in the oxidation of indane and tetralin with hydrogen peroxide, Appl. Catal. A Gen. 366 (2009) 275–281.
[24] N. Mizuno, M. Misono, Heterogeneous catalysis, Chem. Rev. 98 (1) (1998) 199–218.
[25] I.V. Kozhevnikov, Catalysis by heteropoly acids and multicomponent polyoxometalates in liquid-phase reactions, Chem. Rev. 98 (1) (1998) 171–198.
[26] W. Trakarnpruk, K. Rujiraworawut, Oxidative desulfurization of gas oil by polyoxometalates catalysts, Fuel Proces. Tech. 90 (2009) 411–441.
[27] Z.E.A. Abdalla, B.S. Li, A. Tufail, Direct synthesis of mesoporous $(C_{19}H_{42}N)_4H_3(PW_{11}O_{39})/SiO_2$ and its catalytic performance in oxidative desulfurization, Colloids Surf. A Physicochem. Eng. Aspects 341 (2009) 86–92.
[28] A. Pate, V. Brahmkhatri, Kinetic study of oleic acid esterification over 12-tungstophosphoric acid catalyst anchored to different mesoporous silica supports, Fuel Process. Tech. 113 (2013) 141–149.
[29] V. Brahmkhatri, A. Patel, 12-Tungstophosphoric acid anchored to SBA-15: an efficient, environmentally benign reusable catalysts for biodiesel production by esterification of free fatty acids, Appl. Cat. A Gen. 403 (2011) 161–172.
[30] B.B. Dong, B.B. Zhang, H.Y. Wu, X. Chen, K. Zhang, X.C. Zheng, Synthesis, characterization and catalytic evaluation of SBA-15 supported 12-tungstophosphoric acid mesoporous materials in the oxidation of benzaldehyde to benzoic acid, Mater. Res. Bull. 48 (2013) 2491–2496.
[31] K. Li, L. Yana, Z. Zenga, S. Luoa, X. Luoa, X. Liua, H. Guoa, Y. Guo, Fabrication of $H_3PW_{12}O_{40}$-doped carbon nitride nanotubes by one-step hydrothermal treatment strategy and their efficient visible-light photocatalytic activity toward representative aqueous persistent organic pollutants degradation, Appl. Cat. B Environ. 156–157 (2014) 141–152.
[32] Y. Gu, R. Wei, X. Ren, J. Wang, Cs salts of 12-tungstophosphoric acid supported on dealuminated USY as catalysts for hydroisomerization of n-heptane, Catal. Lett 113 (2007) 41–45.
[33] C. Yuan, J. Chen, Preparation of heterogeneous mesoporous silica-supported 12-Tungstophosphoric acid catalyst and its catalytic performance for cyclopentene oxidation, Chin. J. Catal. 32 (2011) 1191–1198.
[34] M. Moritz, M. Łaniecki, SBA-15 mesoporous material modified with APTES as the carrier for 2-(3-benzoylphenyl)propionic acid, Appl. Surf. Sci. 258 (2012) 7523–7529.
[35] X. Wang, Y.-H. Tseng, J.C.C. Chan, S. Cheng, Direct synthesis of highly ordered large-pore functionalized mesoporous SBA-15 silica with methyl aminopropyl groups and its catalytic reactivity in flavanone synthesis, Micropor. Mesopor. Mater. 85 (2005) 241–251.
[36] D. Zhao, J. Feng, Q. Huo, N. Melosh, G.H. Fredrickson, B.F. Chmelka, G.D. Stucky, Triblock copolymer syntheses of mesoporous silica with periodic 50 to 300 angstrom pores, Science 279 (5350) (1998) 548–552.
[37] Q. Dai, X. Wang, G. Chen, Y. Zheng, G. Lu, Direct synthesis of Cerium(III)-incorporated SBA-15 mesoporous molecular sieves by two-step synthesis method, Micropor. Mesopor. Mater. 100 (2007) 268–275.
[38] D.L. Pavia, G.M. Lampman, G.S. Kriz, J.R. Vyvyan, Introduction to spectroscopy, Fourth Edition., Academic Press, Washington, 2009.
[39] X.L. Yang, W.L. Dai, H. Chen, J.H. Xu, Y. Cao, H.X. Li, K.N. Fan, Novel tungsten-containing mesoporous HMS material: its synthesis, characterization and catalytic application in the selective oxidation of cyclopentene to glutaraldehyde by aqueous H_2O_2, Appl. Catal. A Gen. 283 (2005) 1–8.
[40] S.J. Greg, K.S.W. Sing, Adsorption, Surface Area and Porosity, second ed., Academic Press, New York, 1982.
[41] J.E. Castanheiro, I.M. Fonseca, A.M. Ramos, J. Vital, Tungstophosphoric acid immobilised in SBA-15 as an efficient heterogeneo us acid catalyst for the conversion of terpenes and free fatty acids, Micropor. Mesopor. Mater. 249 (2017) 16–24.
[42] X.S. Zhao, G.Q. Lu, A.K. Whittaker, G.J. Millar, H.Y. Zhu, Comprehensive study of surface chemistry of MCM-41 using ^{29}Si CP/MAS NMR, FTIR, pyridine-TPD, and TGA, J. Phys. Chem. B 101 (33) (1997) 6525–6531.
[43] J. Goschnick, M. Frietsch, T. Schneider, Non-uniform SiO_2 membranes produced by ion beam-assisted chemical vapour deposition to tune WO_3 gas sensor microarrays, Surf. Coat. Technol. 108 (109) (1998) 292–296.
[44] I. Jiménez-Morales, J. Santamaría-González, P. Maireles-Torres, A. Jiménez-López, Zirconium doped MCM-41 supported WO_3 solid acid catalysts for the esterification of oleic acid with methanol, Appl. Catal. A Gen. 379 (2010) 61–68.
[45] J. Gil-Rostra, M. Cano, J.M. Pedrosa, F.J. Ferrer, F. Garcia-Garcia, F. Yubero, A.R. Gonzalez-Elipe, Electrochromic behavior of $W_xSi_yO_z$ thin films prepared by reactive magnetron sputtering at normal and glancing angles, ACS Appl. Mater. Interfaces 4 (2012) 628–638.
[46] X. Jiang, H. Li, W. Zhu, L. He, H. Shu, J. Lu, Deep desulfurization of fuels catalyzed by surfactant-type decatungstates using H_2O_2 as oxidant, Fuel 88 (2009) 431–436.